Pure Appl. Geophys. 171 (2014), 2841–2862

DOI 10.1007/s00024-014-0804-0

Pure and Applied Geophysics

Radiated Energy of Great Earthquakes from Teleseismic Empirical Green's Function Deconvolution

Annemarie S. Baltay,[1,3] Gregory C. Beroza,[1] and Satoshi Ide[2]

Abstract—We expand on the empirical Green's function deconvolution method of Ide *et al.* (2011) to estimate radiated energy for the six largest earthquakes worldwide over the last 10 years: 2011 M_w 9.0 Tohoku-Oki, 2004 M_w 9.1 Sumatra, 2010 M_w 8.8 Maule, 2005 M_w 8.7 Nias, 2007 M_w 8.5 Bengkulu, and 2012 M_w 8.6 off-Sumatra. Deconvolution of *P*, *SV* and *SH* components gives consistent energy results that are comparable to estimates found independently by other researchers. Apparent stress for the five great thrust earthquakes is between 0.4 and 0.8 MPa, while the 2012 off-Sumatra strike-slip earthquake has a higher apparent stress of 3 MPa, which is consistent with other studies that find a tendency for strike-slip events to be more energetic. Our results are within the spread of apparent stress from the wider global earthquake population over a large magnitude range. The azimuthal distribution of energy in each case shows signs of directivity, and in some cases, shows less energy radiated in the trench-ward direction, which may suggest enhanced tsunami potential. We find that eGfs as small as ~M 6.5 can be used for teleseismic deconvolution, and that an eGf-mainshock magnitude difference of 1.5 units yields stable results. This implies that M 8 is the minimum mainshock size for which teleseismic eGf deconvolution will work well. We propose that a database of eGf events could be used to calculate radiated energy and apparent stress of great, hazardous events in near real time, i.e., promptly enough that it could contribute to rapid response measures.

1. Introduction

Great earthquakes, $M_w \geq 8.5$, are rare and potentially devastating events. Until the occurrence of the 2004 M_w 9.1 Sumatra earthquake, no broadband digital recordings existed for these very large events, and precise source parameters were unavailable. The 2004 Sumatra event came with surprises: an extended rupture zone of almost 1,300 km in length, and a large tsunami that caught much of the Indian Ocean Basin unprepared (Ishii *et al.* 2005). The 2011 M_w 9.0 Tohoku-Oki earthquake had a much more compact source zone, and in contrast to the 2004 Sumatra event, generated high frequencies at the deep edge of the rupture with slower, higher amplitude slip at the trench, with the latter making an unfortunately large contribution to the devastating tsunami that followed. Although the site of the Tohoku-Oki event was deemed the most likely location for a future magnitude (M) 7.5–8 earthquake, the extent of rupture and magnitude of slip was unanticipated [Lay *et al.* 2013; National Seismic Hazard Maps for Japan (2005), http://www.jishin.go.jp/main/index-e.html]. The 2012 M_w 8.6 off-Sumatra event is the largest strike-slip earthquake ever recorded, and while it caused little damage, it raises the prospect that the maximum possible size of continental strike-slip earthquakes may be underestimated. Because each of these earthquakes is uncommon in the instrumental record, they merit intense study.

Radiated seismic energy is a scalar measure of the strength of an earthquake that can be related to other physical parameters, such as fracture energy, rupture velocity and stress drop. By studying the relationship between radiated seismic energy, a dynamic parameter, and seismic moment, a static measure of the earthquake's size, we can gain insight into the dynamic processes of an earthquake. If all earthquakes follow self-similar physics, then simple power-law scaling will explain earthquake size-

For submission to the special issue of Pure and Applied Geophysics (PAGEOPH), entitled "Earthquake Source Physics on Various Scales."

Electronic supplementary material The online version of this article (doi:10.1007/s00024-014-0804-0) contains supplementary material, which is available to authorized users.

[1] Department of Geophysics, Stanford University, Stanford, CA, USA. E-mail: abaltay@usgs.gov

[2] Department of Earth and Planetary Science, University of Tokyo, Tokyo, Japan.

[3] *Present Address*: United States Geological Survey, Menlo Park, CA, USA.

dependence. If not, then it would point to an intrinsic length scale related to some physical factor controlling the earthquake faulting process. Whether all earthquakes have the same ratio of seismic energy to moment, E_R/M_o, remains an open question (e.g. Boatwright and Choy 1986; Abercrombie 1995; Ide and Beroza 2001; Choy *et al.* 2006; Bormann and Di Giacomo 2011), and how the very largest earthquakes radiate energy is not well understood, due to the fact that great earthquakes are uncommon and it is challenging to measure their energy accurately.

Strike-slip events have been shown to have larger scaled energy than dip-slip events. Choy and Boatwright (1995) estimate an order of magnitude higher scaled energy for strike-slip vs. reverse-faulting events, and Pérez-Campos and Beroza (2001) found this difference to be a factor of five, using a revised method to account for potential biases. Convers and Newman (2011) determine strike-slip events to be twice as energetic as thrust events. The largest strike-slip earthquakes occurring in oceanic lithosphere may be associated with emergent or diffuse plate boundaries, rupturing cold, intact crustal material. The associated earthquakes may have high stress drop and large scaled energy. In contrast, the largest thrust events tend to occur on mature plate boundaries that repeatedly rupture with lower stress drop and scaled energy.

A second class of earthquakes that may display abnormal ratios of E_R/M_o are "tsunami earthquakes", which excite a much larger tsunami than expected for their magnitude (Kanamori 1972). Newman and Okal (1998) found that many of these tsunami earthquakes have anomalously low ratios of radiated energy to seismic moment, which provides a motivation for rapid determination of this source parameter. On the other hand, great earthquakes may be tsunamigenic without being deficient in radiated energy. In either situation, radiated energy provides important information that is highly relevant to understanding both tsunamigenesis and earthquake dynamics.

Estimates of energy for large earthquakes are typically computed by making path corrections to account for attenuation and geometrical spreading, as well as site and surface corrections, using teleseismically recorded data (Boatwright and Choy 1986; Perez-Campos *et al.* 2003; Convers and Newman 2011). Empirical Green's functions have been employed as an effective means for making these corrections for local earthquakes, and avoid the need for explicit determination of path corrections or radiation pattern coefficients. Use of eGfs assumes that a smaller, collocated event, usually at least one magnitude unit smaller, can approximate the point-source response to a double-couple source (e.g. Hartzell 1978; Courboulex *et al.* 1996; Hough 2001; Kane *et al.* 2011). Then, the source time function of the larger mainshock event can be determined by deconvolving the smaller Green's function event from the larger event.

Empirical Green's functions have been used profusely on a local scale (within a few hundred km) to correct to source spectra of earthquakes up to $\sim$M 7 (Venkataraman *et al.* 2002; Ide *et al.* 2003; Baltay *et al.* 2010, 2011); however, for great earthquakes in which the rupture dimension can no longer be considered negligible compared to the source-station distance, the local empirical Green's function assumptions are not met. Ammon *et al.* (1993) showed that teleseismic surface wave deconvolution could work between earthquakes of magnitude 7.2 and 7.4 with eGf events of magnitude $\sim$6 to resolve fault finiteness. When considered at teleseismic distances ($\Delta > 30°$), even very large ruptures can be considered point sources, which leads us to consider large earthquakes ($\sim$M 6.5–7.5) as empirical Green's functions, to correct for path and site effects of great earthquakes.

In this study, we expand the teleseismic eGf deconvolution approach (Ide *et al.* 2011) to model source spectra of the six recent great earthquakes. We can accurately estimate the radiated seismic energy using either *P* or *S* wave groups, and find the scaled energy, E_R/M_o, to be fairly consistent for the five thrust events, and about a factor of five larger for the 2012 off-Sumatra strike slip event. Our estimates of E_R are consistent with those from previous teleseismic studies of great earthquakes, and the higher energy associated with the 2012 off-Sumatra strike slip event is in agreement with the mechanism dependence shown in previous studies (Choy and Boatwright 1995; Pérez-Campos and Beroza 2001; ConversNewman 2011). With the dense azimuthal coverage of the global seismic network (GSN), we find that some of the events, especially the 2011 Tohoku-Oki earthquake, have strong directivity, consistent with the known direction of rupture. Others show less clear azimuthal dependence, such as the 2007

Bengkulu earthquake, or no variation with azimuth, as in the case of the 2012 off-Sumatra event, which ruptured multiple conjugate fault planes. We find at least a factor of two, and up to an order of magnitude, difference in energy from maximum to minimum with some events, implying that directivity effects should be considered when estimating energy teleseismically. Finally, we suggest that this teleseismic eGf deconvolution could be adapted for use in real time, for rapid characterization of the dynamic properties of an earthquake, as also pointed out by Di Giacomo *et al.* (2010) and Convers and Newman (2011). An eGf catalog could be built of preprocessed eGf events for all regions in the world that are available, covering most of the regions that are most likely to host a great earthquake in the future. Since so little is known about the great, hazardous events, any information discerned quickly after the occurrence of an event has the potential to aid in rapid response.

2. *Teleseismic eGf Deconvolution*

We consider six great earthquakes recorded worldwide over the past 10 years: 2011 M_w 9.0

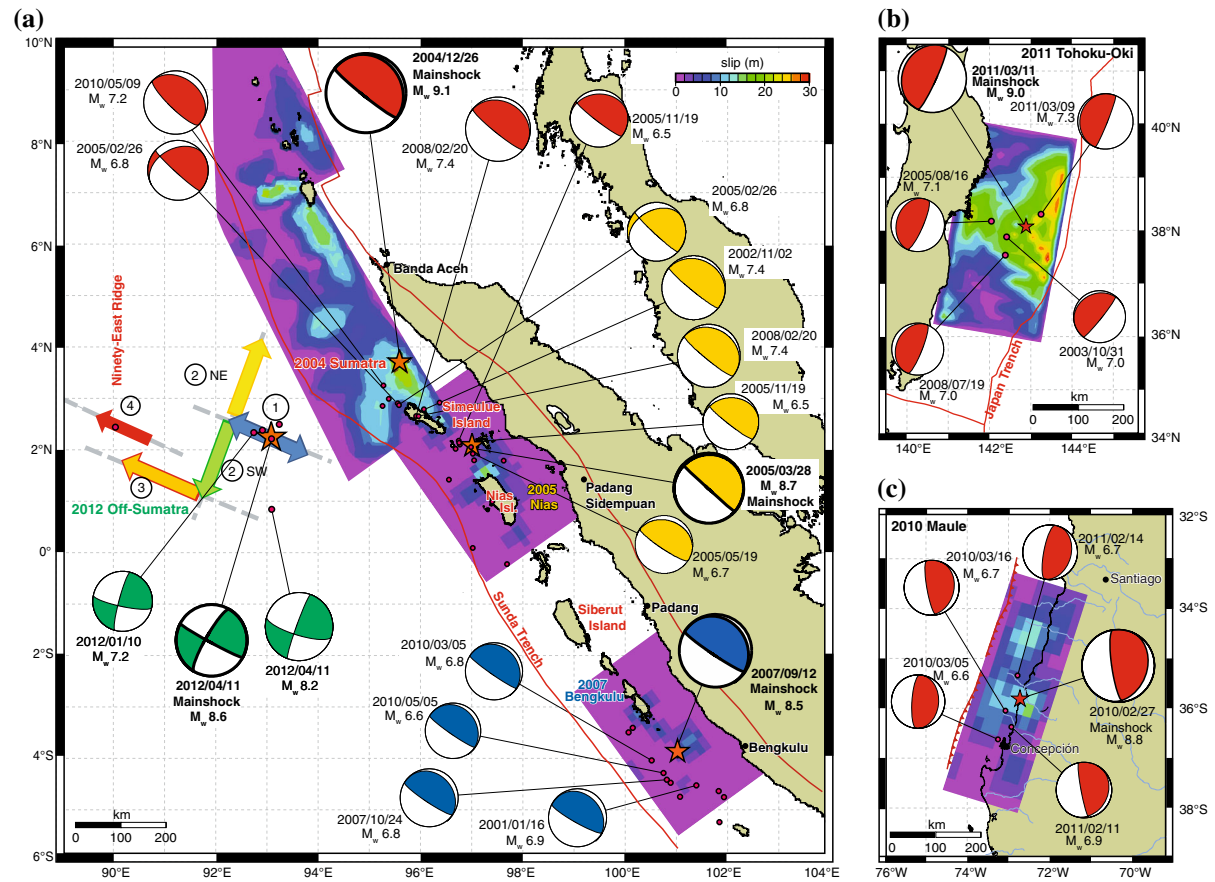

Figure 1

Maps of great earthquake locations, rupture history and gCMT locations and mechanisms of candidate eGf earthquakes. **a** Greater Sumatra map, showing: 2004 Sumatra earthquake and eGf events (*red* focal mechanisms), slip distribution from Ammon *et al.* (2005); 2005 Nias earthquake and eGf events (*yellow* focal mechanisms), slip distribution from Konca *et al.* (2007); 2007 Bengkulu earthquake and eGf events (blue focal mechanisms), slip distribution from Konca *et al.* (2008); and 2012 off-Sumatra earthquake and eGf events (*green* focal mechanisms), schematic of rupture propagation from Meng *et al.* (2012), who model the rupture as starting at (*1*), rupturing bi-laterally along the *blue arrow* before moving to a conjugate fault and rupturing again bilaterally to the northeast (*yellow arrow*) and southwest (*green arrow*) at the (*2*)s, then moving again to a conjugate fault at (*3*), *orange arrow*, before jumping to a parallel plane shown with the *red arrow* at (*4*). **b** Map of 2011 Tohoku-Oki rupture area and candidate eGf events. Slip distribution from Ide *et al.* (2011). **c** Map of 2010 Maule rupture area and candidate eGf events. Slip distribution from Hayes (2010) USGS Teleseismic model, as displayed by Moreno *et al.* (2010)

Tohoku-Oki, 2004 M_w 9.1 Sumatra, 2010 M_w 8.8 Maule, 2005 M_w 8.7 Nias, 2007 M_w 8.5 Bengkulu, and 2012 M_w 8.6 off-Sumatra, and nearby large earthquakes from M ~6.0 to ~7.9 as potential empirical Green's functions (Fig. 1). We estimate the energy of each mainshock by deconvolution of several candidate eGfs located near the mainshock, and with similar mechanism to that of the mainshock. The eGfs considered occur both before and after the mainshock, except for the 2004 Sumatra and 2010 Maule eGfs, which are all afterwards.

We use both *P* and *S* waves recorded by broadband global seismic stations in the GSN. For both the mainshock and eGf events, we analyze vertical (BHZ) records, windowed from 90 s before the *P* arrival to 360 s after, and *S*-horizontal components (BHE and BHN), rotated to radial (SV) and transverse (SH) directions and windowed from 90 s before the *S* arrival to 360 s after. We use recordings from stations of distance $\Delta = 30°$ to $\Delta = 90°$, which have relatively simple propagation characteristics because their turning points are in the lower mantle. This combination of window length and recording distance were chosen to maximize the signal of the *P* and *S* waves separately, without contamination of too many other phases. Closer than 30°, *P*-wave windows will contain *S*-waves within 270 s, and triplication of arrivals from upper mantle structure and reflected *PP* energy complicate the record; Beyond 90°, there is a loss of energy as body waves diffract around the earth's core. *P*, *pP*, and *sP* waves will all be contained in the vertical component, but for shallow earthquakes, these phases have nearly the same path, and hence arrive together to create a coherent wave package that can be analyzed together.

We taper the time series over the 90 s before the arrival and the 90 s of the end of the window (from 270 to 360 s), so that 270 s of record with no tapering are used, and calculate the spectrum of each component at each station. We smooth each spectrum into 90 bins that are evenly spaced in log frequency from 1 mHz to 10 Hz. Figure 2 shows example windowed *P* and *S* waveforms at one global station, KEV, for the 2011 Tohoku-Oki earthquake, and the four candidate eGf events.

We correct both the mainshock and eGf spectra together, such that the corrected spectrum of the eGf is an ideal Brune ω-squared model, as in Baltay *et al.* (2010), using the USGS centroid moment given in Tables 1, 2, 3, 4, 5, and 6 and a reference stress drop of 3 MPa to define the corner frequency. We follow Hanks and Thatcher (1972) and assume $\beta = 3{,}600$ m/s, so that corner frequency is,

$$f_c = \left(\frac{\Delta\sigma}{8.47M_o}\right)^{1/3}\beta. \quad (1)$$

In log–log frequency space, deconvolution of the time series is equivalent to subtraction of the eGf spectra from the mainshock spectra. In the deconvolution (subtraction), the correction is the same for both the eGf and the mainshock at each frequency, so that the relative spectral levels between the two events are maintained. We set the absolute moment level of all spectra based on the moment of the eGf from the USGS Centroid Moment Tensor (Fig. 4a). We then compare all of the mainshock spectra to investigate their low-frequency behavior. The frequency at which all the mainshock spectra, as measured at the various stations, converge is chosen as the low frequency cutoff for that eGf event, maximizing the coherency. This point is usually near 10 mHz (100 s), and represents the lowest frequency at which the eGf recording is above the noise, and the lowest frequency at which we use direct data for the mainshock spectrum.

Although we can measure the eGf spectrum down to the low-frequency cutoff near 10 mHz (100 s), the long-period moment level of the mainshock is not completely captured at these periods, due to the exceptionally long rupture durations of great earthquakes. The duration of the events we have studied range from 100 s for the 2007 M_w 8.5 Bengkulu earthquake (Konca *et al.* 2008) to over 500 s for the 2004 M_w 9.1 Sumatra event (Lay *et al.* 2005). For this reason, we extrapolate the mainshock spectrum to lower frequencies following an ω^{-2} trend, until the independent moment of both the eGf and mainshock are recovered, at a frequency of about 1–4 mHz (depending on the event, eGf and component). Figure 4 (and Figs. S2a–b, S4a–b, S6a–b, S8a–b and S10a–b) shows the extrapolated part of the spectra in thin lines. Because the eGf spectra are unstable below about 100 s, we are unable to adequately correct the mainshock for these very low frequencies. It is also

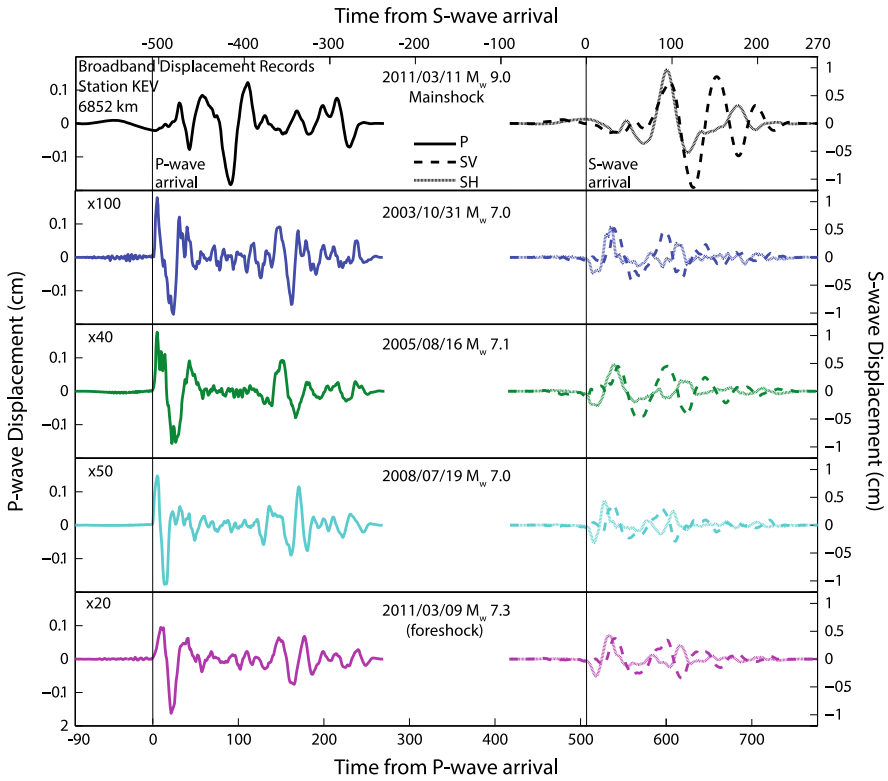

Figure 2
Broadband displacement waveforms from 2011 Tohoku-Oki mainshock (*top panel*) and four candidate eGf events, recorded at station KEV with a distance of 6,852 km. *Left* seismograms are *P*-wave vertical recordings, *right* are the SV and SH components, each windowed from 90 s before the first arrival to 270 s afterwards, and tapered. The eGf recordings are scaled by a factor ranging from 20× to 100×, shown in the *upper left corner* of each panel

Table 1

Radiated seismic energy of the 2011 M_w 9.0 Tohoku-Oki earthquake, corrected by each eGf, with given eGf moment and magnitude

Catalog information				Radiated energy (J $\times 10^{17}$)						
#	Date (Y/M/D)	M_o (Nm, $\times 10^{19}$)	M_w	*P*	SV	SH	Average	min	max	*N*
4	2003/10/31	3.4	7.0	12.19	9.58	10.58	10.73	9.14	12.59	28
6	2005/08/16	4.7	7.1	6.56	5.25	5.84	5.86	5.07	6.77	27
9	2008/07/09	3.8	7.0	7.90	6.50	6.59	6.97	6.03	8.06	32
10	2011/03/09	9.9	7.3	7.58	4.88	4.89	5.66	5.19	6.16	41
Average of each component				8.32	6.32	6.68				
Average of S-components					6.50					
Overall average							7.06	6.58	7.57	368

The $\log_{10}$ average is weighted azimuthally. *N* is the number of stations recording each eGf event (note that not all components at each station are always used, so that the sum of all components at all stations may be less than 3**N*). The min and max are the aleatory 95 % confidence intervals based on the $\log_{10}$ distribution of the energy estimates at individual stations. The 95 % confidence intervals are equal to $\pm 2 * \log_{10}$ standard error (the data sample standard deviation over all three components and all *N* station divided by the square root of *N**3). They are symmetric in $\log_{10}$ space, and hence asymmetric in linear space, as presented here

possible that teleseismic spectra are deficient in low-frequency energy in the time window considered, due to possible interference effects from free surface reflections (Kanamori and Given 1981). This extrapolation accounts for only about 10–20 % of the total energy of the mainshock, depending on the

Table 2

Radiated seismic energy of the 2004 M_w 9.1 Sumatra earthquake

Catalog information				Radiated energy (J $\times 10^{17}$)						
#	Date (Y/M/D)	M_o (Nm, $\times 10^{19}$)	M_w	*P*	SV	SH	Average	min	max	*N*
2	2005/02/26	1.7	6.8	8.93	12.91	9.37	10.26	9.39	11.21	45
4	2005/11/19	0.62	6.5	6.52	9.48	6.67	7.45	6.73	8.23	41
5	2008/02/20	11	7.4	5.08	7.37	8.02	6.70	6.08	7.37	36
7	2010/05/09	8.5	7.2	4.46	6.38	5.56	5.41	4.72	6.20	36
Average of each component				6.03	8.71	7.27				
Average of S-components					7.96					
Overall average							7.25	6.84	7.69	463

Columns as described for Table 1

Table 3

Radiated seismic energy of the 2010 M_w 8.8 Maule earthquake

Catalog information				Radiated energy (J $\times 10^{17}$)						
#	Date (Y/M/D)	M_o (Nm, $\times 10^{19}$)	M_w	*P*	SV	SH	Average	min	max	*N*
1	2010/03/05	0.73	6.6	1.39	0.92	1.12	1.13	1.01	1.27	35
2	2010/03/16	1.20	6.7	2.28	1.80	1.77	1.93	1.72	2.17	35
4	2011/02/11	5.30	6.9	3.92	2.48	2.06	2.72	2.41	3.06	31
5	2011/02/14	1.70	6.7	2.92	1.78	1.57	2.01	1.75	2.32	30
Average of each component				2.45	1.65	1.59				
Average of S-components					1.62					
Overall average							1.86	1.74	1.99	383

Columns as described for Table 1

Table 4

Radiated seismic energy of the 2005 M_w 8.7 Nias earthquake

Catalog information				Radiated energy (J $\times 10^{17}$)						
#	Date (Y/M/D)	M_o (Nm, $\times 10^{19}$)	M_w	*P*	SV	SH	Average	min	max	*N*
2	2002/11/02 01:26:10	13	7.4	2.56	2.69	2.26	2.49	2.32	2.68	52
4	2005/02/26	1.7	6.8	3.28	4.08	3.46	3.59	3.42	3.77	64
8	2005/05/19	1.2	6.7	2.07	1.62	1.52	1.72	1.63	1.82	62
10	2005/11/19	0.62	6.5	1.98	1.85	1.58	1.80	1.70	1.89	57
13	2008/02/20	11	7.3	2.15	1.77	1.63	1.84	1.66	2.03	44
Average of each component				2.36	2.25	1.98				
Average of S-components					2.11					
Overall average							2.19	2.11	2.28	819

Columns as described for Table 1

station and eGf used (Fig. 4b), which is less than the variability of ±0.2 magnitude units in energy magnitude quoted in other studies (i.e. Di Giacomo *et al.* 2010). The close correspondence of the mainshock spectra to each other, when corrected by different eGf events, indicates that the corrected source spectra and

Table 5

Radiated seismic energy of the 2007 M_w 8.5 Bengkulu earthquake

Catalog information				Radiated energy (J $\times 10^{17}$)						
#	Date (Y/M/D)	M_o (Nm, $\times 10^{19}$)	M_w	*P*	SV	SH	Average	min	max	*N*
4	2001/01/16	2.0	6.8	1.66	1.05	1.28	1.31	1.18	1.45	46
6	2007/10/24	2.3	6.9	1.56	0.88	0.73	1.00	0.89	1.12	57
9	2010/03/05	1.6	6.8	2.00	1.45	1.12	1.48	1.36	1.62	55
10	2010/05/05	0.8	6.6	2.20	1.41	1.32	1.60	1.44	1.78	50
Average of each component				1.84	1.17	1.08				
Average of S-components					1.13					
Overall average							1.33	1.26	1.40	608

Columns as described for Table 1

Table 6

Radiated seismic energy of the 2012 M_w 8.6 off-Sumatra earthquake, corrected by the Mw 7.2 eGf

Catalog information				Radiated energy (J $\times 10^{17}$)						
#	Date (Y/M/D)	M_o (Nm, $\times 10^{19}$)	M_w	*P*	SV	SH	Average	min	max	*N*
4	2012/01/10	7.2	7.2	8.03	6.17	6.09	6.71	5.24	8.59	57
Average of S-components					6.13					
Overall average							6.71	5.24	8.59	164

Columns as described for Table 1

extrapolation to low frequencies are robust with respect to the eGf choice.

Once we calculate corrected displacement source spectra from eGf deconvolution, we further extrapolate the spectra to the high and low frequencies following the Brune ω-squared model (similar to illustration in BALTAY *et al.* 2010; Fig. 1d). The low frequency point near 1–4 mHz at which the mainshock spectrum reaches the moment level is taken as an effective corner frequency, below which the spectrum is extrapolated along the flat, moment, part of the spectrum, to frequencies less than 0.1 mHz. In this high frequency range, the spectrum is extrapolated as ω-squared to frequencies greater than 100 Hz. Figure 4 fully illustrates these limits, with the thick lines representing the range of the eGf events, the thin lines in Fig. 4a the extrapolation to the moment level, and finally, the cumulative curve in Fig. 4b showing the large range over which the integration is performed.

Radiated energy is proportional to the integral of the corrected velocity spectra squared,

$$E_R = \frac{I}{4\pi^2 \rho \beta^5} \int_0^\infty \left| \omega \cdot \dot{M}(\omega) \right|^2 d\omega, \quad (2)$$

where $\dot{M}(\omega)$ is the moment rate (displacement) spectrum, $\beta = 3.6$ km/s, $I = 2/5$ and $\rho = 3{,}000$ kg/m^3. We estimate E_R for the mainshock as corrected by each eGf event, and for each of three components of motion, at each GSN station. Although we use both *P* and *S* wave, the relative eGf deconvolution yields similar source spectra (i.e., Fig. 4a) and hence the single Eq. (2) is valid to calculate the energy, regardless of the component. We also calculate scaled energy and apparent stress after WYSS and BRUNE (1968),

$$\tau_a = \mu \frac{E_R}{M_o}, \quad (3)$$

with the shear modulus $\mu = 39$ GPa, using $\mu = \rho\beta^2$.

3. Choice of Empirical Green's Function

While our use of large, teleseismic empirical Green's functions in this study allows us to calculate

radiated seismic energy from the largest earthquakes, the method is not without some of the limitations that also affect local and regional eGf deconvolution. Typically, it is considered that the eGf event should be (1) small enough in comparison to the main event to approximate a point-source; (2) close enough to the main event so that path effects are similar; and (3) of similar focal mechanism so that the radiation patterns of the eGf and main event are similar. The choice of eGf events can be a source of apparent variability in the spectral signature of the main event, and deviations from the conditions above can introduce errors in the parameters estimated for the main event (e.g., Kane *et al.* 2013; Mori and Frankel 1990; Abercrombie 2013). Kane *et al.* (2013) determined that the most important criteria for an eGf event is co-location to the mainshock. They suggest an optimal eGf-mainshock separation distance of about 1 km for events with radius $\sim$0.1 km when observing at local distances ($\sim$10 km); extending these ratios to teleseismic recording distances (3,000–10,000 km) and great earthquake dimensions (tens of km radius) implies an eGf-mainshock separation of $\sim$100 km is reasonable. Kane *et al.* (2013) also suggest that eGf size in relation to the mainshock and similarity of mechanism are important. Because teleseismic eGf deconvolution to estimate seismic energy has not been undertaken before, we test some of these assumptions.

In the 2005 M_w 8.7 Nias and 2007 M_w 8.5 Bengkulu data sets, we consider up to 14 possible eGf events each, ranging from M_w 6.0 to M_w 7.8, with normal and strike-slip mechanisms, as well as thrust events that match the mechanism of the mainshock. The locations are spread throughout the fault plane. We use these events to test the limitations on the choice of eGf. For the events considered, the $\log_{10}$ standard deviation of the mainshock energy determined using all potential eGf events is 0.25 (2005 Nias) and 0.40 (2007 Bengkulu). With just the chosen eGf events, shown in Tables 4 and 5, the $\log_{10}$ std drops to 0.14 and 0.09, showing that the correct choice of eGf events gives much more stable and reliable mainshock energy estimates.

We find that anything less than $\sim$M 6.5 is too small to use as an eGf, at least for teleseismic distances, and that energy results determined with these eGfs are systematically smaller than the average (Fig. 3; Events 5, 7 and 8). Events of this size have peak amplitudes near 10^{-6} m/s (vertical) at teleseismic distances, and corner frequencies near 0.1 Hz. Microseismic noise has a peak at 8 s, with a median amplitude of about 3×10^{-7} m/s (Aster *et al.* 2008), and hence the eGfs of M $< \sim$6.5 are too close to the microseismic background noise, and may display artificially elevated amplitudes. When these events are used as eGfs, the corrected mainshock spectrum is biased towards low amplitude in the microseismic band, and leads to lower estimates of radiated energy.

We also consider events as large as M_w 7.8–7.9 as potential eGfs. A rule of thumb for choosing an appropriate eGf is a magnitude separation of 1.5 units between the mainshock and eGf (e.g. Courboulex *et al.* 1996; Hough 2001; Kane *et al.* 2011). In the case of the 2005 M_w 8.7 Nias, we find that the largest potential eGf (M_w 7.8 2010/04/06) is too large to be used as an eGf for this event, with a magnitude difference of only 0.9. Our teleseismic eGf deconvolution method is very sensitive to relative spectral amplitudes, and it is possible for the large eGfs to have amplitudes as high or higher than the mainshock at some frequencies, which leads to unstable, unreliable radiated energy estimates. Event 11 shown in Fig. 5 from the Bengkulu sequence is actually the October 2010 M_w 7.8 tsunami earthquake, with depleted radiated energy when compared with a typical earthquake of its magnitude (Lay *et al.* 2011; Newman *et al.* 2011). Therefore, we would expect its spectra to have lower amplitudes than the ideal Brune spectra to which it was corrected. This gives rise to corrected mainshock spectra that are enhanced in energy, and thus an overestimated value of radiated energy. Because this event is known to be an enervated tsunami earthquake, it is not ideal to use as an eGf, and emphasizes the need for careful eGf selection.

To test the assumption of like mechanisms and locations, we consider potential eGfs with differing mechanisms and locations. We find that mainshock energies estimated using eGfs of similar location and mechanism (shallow thrust) have much smaller interstation standard error, shown by error bars in Fig. 3. These are the results used in the final analysis. While eGfs with a normal sense of motion yield mainshock

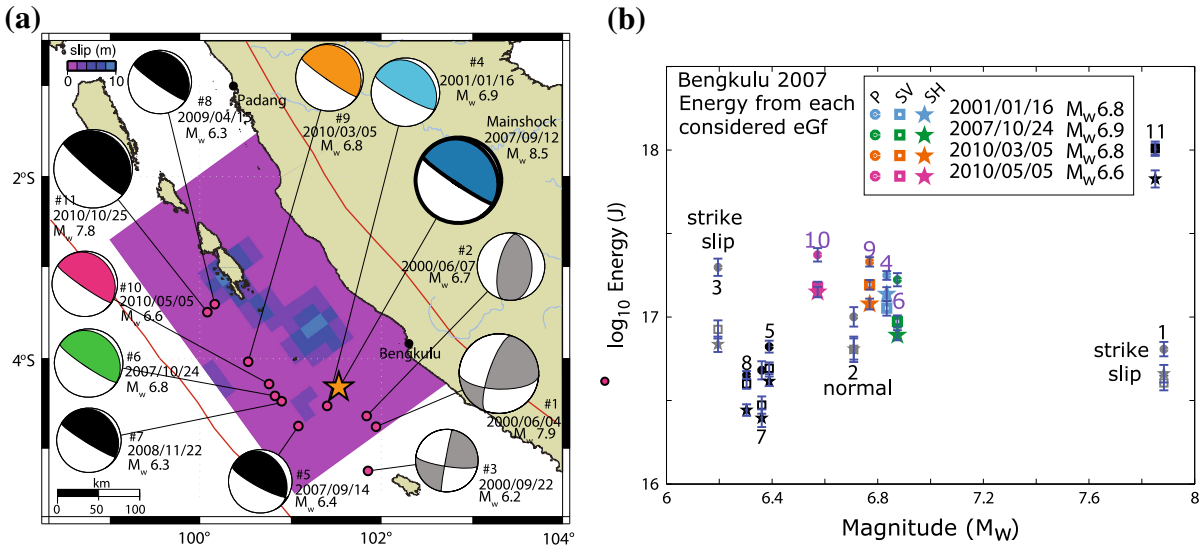

Figure 3

a Map showing location, size and mechanism of the 11 potential eGf events and **b** three components of radiated energy of the M_w 8.5 Bengkulu mainshock, as measured by the 11 different considered eGfs. Shown in *colors* are the four eGfs used in the analysis (#4, #6, #9, #10). Estimates from each of three components are shown in different *symbols* (*P*-wave *vertical* in *circles*; SV in *squares*; and SH in *stars*). *Blue bars* show standard error of the estimate using inter-station standard deviation. Event 1 is strike slip and gives greater variability between station measurements (*larger error bars*); Event 11, ~M 7.9, is the October 2010 tsunami earthquake, and is hence depleted in energy, so that its use as an eGf gives artificially elevated mainshock energy. Event 2 is discarded due to its opposite (normal) mechanism. Events 3, 5, 7 and 8 are too small, and hence underestimate the mainshock energy. In most cases, the *P* wave gives slightly higher radiated energy estimates, but all three components yield similar results

energies consistent with the average, the azimuthal distribution of energy determined by a normal eGf is more strongly variable (larger error bars in Fig. 3; Event #2). Strike-slip eGfs yield highly variable estimates of mainshock energy compared to the other events because the corrected mainshock spectra are less unstable, while eGFs with mechanisms consistent with that of the mainshock yield robust and stable results.

In the 2005 Nias sequence, we test a M_w 6.8 with a very similar mechanism to that of the mainshock, but located much closer to the trench and nearly 150 km from the area of high slip. Mainshock energy estimated from this eGf has the highest inter-station standard error of any considered thrust eGf. We find that eGfs close to the epicenter (within ~100 km) yield energy estimates with less variation between *P* and *S* components, as well as smaller inter-station standard error.

Also of interest is the effect of depth of the eGf event. However, the events considered here as potential eGfs are all located at similar depths between 21 and 36 km, on the subducting plate interface. Most of the events are located not far from the areas that ruptured in the main event, as can be seen in Fig. 3a. Due to the lack of diversity in depth, we don't see any correlation between the eGf quality and depth. We may expect to see an effect if eGf events were significantly deeper or below the subduction plate interface, or if they were very shallow in the wedge. It is also possible that at teleseismic distances, the depth is a less important factor, as compared to the mechanism, magnitude and location. Hence, we conclude that a radius of 100 km is the upper limit for mainshock-eGf distances, within which eGfs provide stable radiated energy estimates for the range of magnitudes we are working with.

4. Radiated Energy from Six Recent Great Earthquakes

For each of the six recent great earthquakes, we consider as many as 14 different empirical Green's function events, and use as many as five for the final analysis (Tables 1, 2, 3, 4, 5, 6). In each case, there is

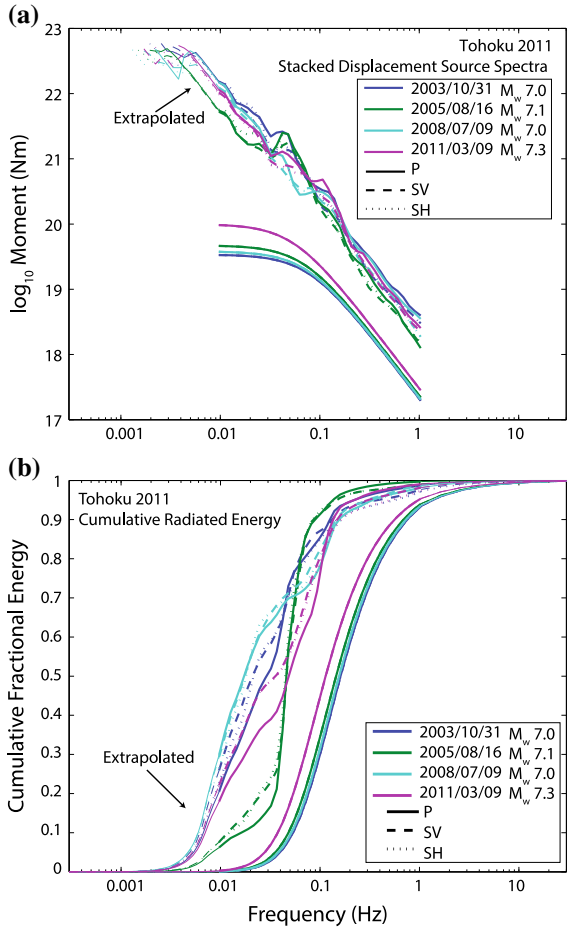

Figure 4

a 2011 Tohoku-Oki displacement source spectra for each eGf, and for the mainshock after deconvolving the different eGf events, stacked over all stations. **b** Cumulative fractional energy of the mainshock corrected individually by each eGf, and stacked over all stations. *Light lines* in the low frequencies of the mainshock in (**a**) and (**b**) show the missing, extrapolated energy, which amounts to ~10–20 % on average

close correspondence between the mainshock spectra when corrected by different eGfs, indicating that the corrected source spectra are robust with respect to the assumed eGf (Fig. 4a, S2a, S4a, S6a, S8a, S10a). By examining the cumulative fractional energy of the mainshock at each frequency, we find that the extrapolated energy is very small in some cases, and at most accounts for ~20 % of the total energy (Figs. 4b, S2b, S4b, S6b, S8b, S10b). In studies of smaller earthquakes, the energy integral is routinely extrapolated to higher frequencies (e.g. Baltay *et al.* 2010). In the case of great earthquakes, however, we are able to measure the high frequency end of the energy spectrum quite well, due to their exceptionally low corner frequencies. The modest extrapolation we perform results in a smaller percentage correction than is typically the case for smaller earthquakes.

We also indicate in thin lines (Fig. 4) the part of the mainshock spectra that has been extrapolated into the low frequencies, below the low cut-off of the eGf, usually near 100 s. For an ideal Brune ω^{-2} spectrum, 80 % of the energy is at frequencies up to 6.25 times the corner frequency (e.g., Singh and Ordaz 1994). For these very large events with corner frequencies of several hundred seconds, that value is well below our 1 Hz high frequency cutoff, so we are measuring most of the radiated energy.

We find that analysis of *P*, *SV* and *SH* waves give very similar mainshock corrected spectra and energy values, and that the two *S*-wave energies are even closer in value, emphasizing the precision of the energy estimates. In many cases, the energy we estimate from the *P* wave is slightly higher. Boatwright and Choy (1986) use primarily *P*-wave spectra for energy determination because *S* waves are strongly attenuated at teleseismic distances. Due to the extremely low frequencies of great earthquakes, the effects of attenuation are manageable, and allow us to make use of *S* waves, essentially tripling the available data.

For all the events, we study the azimuthal dependence of the radiated energy. Empirical Green's functions correct the mainshock for radiation patterns, but not for azimuthal variation due to the effect of source-finiteness. The eGf events are much smaller and do not display strong directivity at the periods we consider. The azimuthal distribution of mainshock energy is thus a source-finiteness effect. To avoid a bias in the station-averaged total radiated energy due to uneven station distribution azimuthally, we bin the station measurements into groups every 30° of azimuth. The final energy estimates for each event represent this azimuthally binned average, so that no cluster of nearby stations (in Europe or North America, for example) has too large an effect on the final radiated energy value.

Lastly, we quantify the aleatory variability of each final energy estimate. For each eGf correction, the energy estimate is made for three components at

between 25 and 60 stations, and these estimates are then averaged to find the overall estimate of the radiated energy for the great earthquake. The minimum and maximum values quoted in Tables 1, 2, 3, 4, 5, 6 are 95 % confidence intervals on the average energy value, determined as ± twice the $\log_{10}$ standard error of the estimate, where the standard error is the ratio of the standard deviation of all the estimates (for all components and stations) and the square root of the number of records. We translate this $\log_{10}$ value into linear space in the table for ease of reading. While this 95 % confidence interval gives us valuable information about how stable each estimate is, it represents only the confidence within our method of the mean value dependent on different observations, and can yield no information about the epistemic uncertainty that is associated with our lack of knowledge about the true model or underlying processes of earthquakes. In this sense, some of the other tests we have considered, i.e., for choice of eGf, comparison to previous studies, contrasting the azimuthal variations or different energy values from the three components, or understanding the shortcomings of the spectral extrapolation of the mainshock into the low frequencies, may give a more enlightened view of the uncertainty associated with our estimates.

4.1. 2011 M_w 9.0 Tohoku-Oki

The M_w 9.0 Tohoku-Oki earthquake of 2011 occurred on March 11 offshore of Honshu, Japan, on the Japan Trench. The earthquake lasted about 160 s, on a rupture plane of about 240 km down dip × 440 km along strike of 200°, with prodigious shallow slip at the trench that generated a large tsunami (Fig. 1) (Ide *et al.* 2011). Waveforms from the four eGf events show very similar patterns in both the *P* and *S* waves. It is apparent from the source time function that the mainshock initially developed slowly, before rapidly increasing in size about a minute after the origin time (Fig. 2). The event was unusual in that it occurred on a compact rupture plane for an event of this size, but also had large, slow shallow slip coupled with deep slip that generated strong high frequency radiation (e.g., Ide *et al.* 2011; Suzuki *et al.* 2011; Koper *et al.* 2011).

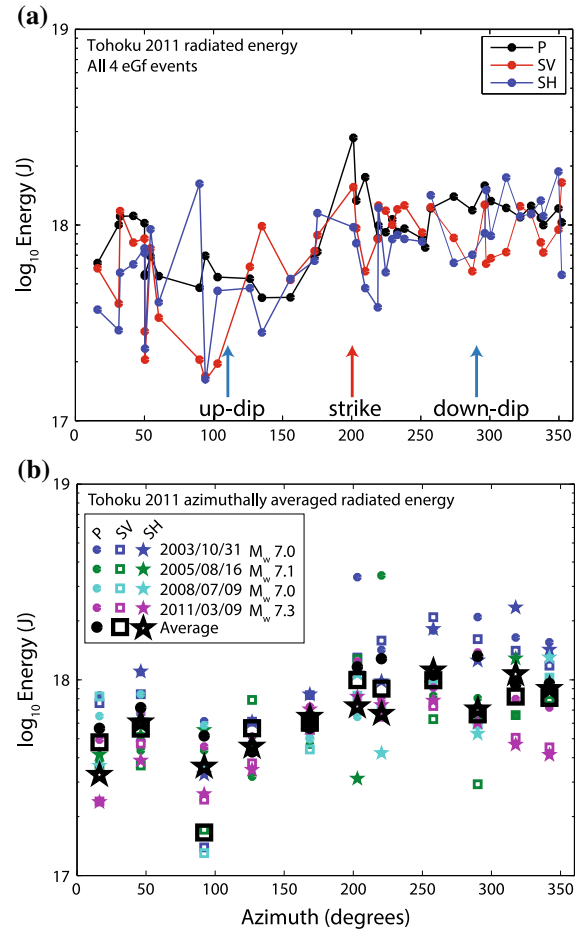

Figure 5
Mainshock radiated energy as a function of station azimuth. **a** Log_{10} average over all eGfs, for each component, shown at all stations. **b** Energy shown as corrected from each eGf event and each component, azimuthally binned every 30°. Average of each bin shown in *black*, used for the final reported energy estimate. Different components shown with different *symbol shapes*

We find a radiated energy of 7.06×10^{17} J, a scaled energy of $E_R/M_o = 1.57 \times 10^{-5}$, and an apparent stress of 0.61 MPa (Table 1). This event shows strong directivity in radiated energy, with a minimum near 100° and a maximum near 200° (Fig. 5). This corresponds to energy directivity found by Convers and Newman (2011), Newman (2011): http://geophysics.eas.gatech.edu/anewman/research/RTerg/. Our cumulative energy shows that the extrapolated energy into the low frequencies is around 10–20 % on average, and that about 90 % of the energy is radiated below 0.1 Hz (Fig. 4).

4.2. 2004 M_w 9.1 Sumatra

The 2004 M_w 9.1 Sumatra earthquake was the first great earthquake to test the GSN. It generated a devastating tsunami, which was made worse by the lack of a tsunami warning system for the Indian Ocean Basin. The earthquake lasted for nearly 500 s, almost three times as long as the Tohoku-Oki event, and its rupture length was the greatest ever recorded—nearly 1,300 km along strike, with a variable slip distribution from the epicenter in the south to the northern tip of the rupture (Ammon *et al.* 2005; Lay *et al.* 2005; Chlieh *et al.* 2007). This event may have had a large slow slip component, releasing energy for up to 1 h after the initiation (Ammon *et al.* 2005; Bilham 2005; Banerjee *et al.* 2005; Lay *et al.* 2005).

Even at teleseismic distances, the 2004 Sumatra earthquake, with its unusually long rupture plane, may not be able to be modeled using a single eGf event; however, Ammon *et al.* (2005) demonstrated that much of the slip occurred in the first 230 s, on the southern-most 420 km of the fault plane (Fig. 1). Since we use the first 270 s of *P* and *S* arrivals, we should capture this initial intense rupture, and be able to model that contribution to the source spectrum from single event eGf deconvolution, provided that the eGfs are located near the patches of high slip. This part of the rupture was along a plane approximately 420 × 240 km, with a strike of about 330°, and average slip of 7 m, compared to 2–5 m average slip on the northern parts of the fault. There are four events with similar mechanism to the mainshock, occurring very near the location of high slip. While the four eGf events have consistent, impulsive arrivals, the mainshock, like the Tohoku-Oki earthquake, is less impulsive and has an obviously longer duration overall (Fig. S1).

We find the energy of the 2004 Sumatra event to be 7.19×10^{17} J, with a scaled energy of 1.12×10^{-5}, and apparent stress of 0.43 MPa, which is slightly less than that of the Tohoku-Oki event (Table 2). The *S* components of the corrected mainshock have more energy in the higher frequencies than do the *P* components, which can also be seen in the cumulative energy (Figure S2b). It is possible that the 270 s window we use around the *S*-wave arrival is also capturing other *P* arrivals due to the long rupture length, which would affect the frequency content. About 80 % of the mainshock energy is below 0.1 Hz.

The 2004 Sumatra event also shows strong directivity in radiated energy, which is expected due to the long and narrow fault plane that ruptured nearly unilaterally to the north (Fig. S2c–d). This directivity is consistent with that found for Rayleigh wave amplitudes, with a large peak towards ~270°–320°, a smaller peak near 20°, and a minimum around 135° (Ammon *et al.* 2005). Although Kanamori (2006) states that there is little directivity effect in his estimation of radiated energy from the 2004 Sumatra earthquake, the stations that he uses show similar energy results. By including more stations, we can better resolve the signature of azimuthal variability in radiated energy.

4.3. 2010 M_w 8.8 Maule

The 2010 M_w 8.8 Maule earthquake occurred along the Chilean subduction zone, just to the north of the 1960 Chilean M_w 9.5 megathrust event (Moreno *et al.* 2010). The rupture occurred on a plane about 150 km along-dip, up to the trench, by 400 km along strike, in NNW direction, and lasted 150 s (Hayes 2010). This event caused a tsunami, but of smaller amplitude than either the 2004 Sumatra or 2011 Tohoku-Oki tsunami. We identify four potential empirical Green's functions near the area of high slip, and discard one due to its distance from the epicenter. The 2010 Maule mainshock shows somewhat more impulsive arrivals, compared to the 2004 Sumatra and 2011 Tohoku-Oki earthquakes, yet the eGf events are even more impulsive (Fig. S3).

We find a radiated energy of 1.86×10^{17} Joules, $E_R/M_o = 1.03 \times 10^{-5}$ and $\tau_a = 0.40$ MPa, averaged over all four eGf events and three components (Table 3). The mainshock source spectra contain a consistent bump near 0.1 Hz that we interpret as a source effect (Fig. S4a). About 20 % of the total energy is from extrapolation to low frequencies, below 10 mHz. The three components of motion show a similar pattern as a function of azimuth, with a minimum of radiated energy towards the southwest, at about 250°, but the azimuthal variation is not as strong as that for the two larger events (Fig. S4c–d).

4.4. 2005 M_w 8.7 Nias

The 2005 M_w 8.7 Nias earthquake occurred south of the 2004 M_w 9.1 Sumatra, along the Sunda trench. The rupture plane is about 150 km wide and 300 km along strike, to the NNW. The event lasted about 120–150 s, and ruptured bilaterally, to the north and south, in two distinct patches (Konca *et al.* 2007). The rupture did not come as close to the trench as the 2004 Sumatra event, however, and generated a much smaller, local tsunami (Dean *et al.* 2010). In this case, we consider 14 different eGf events, but discard most of them to use five earthquakes, occurring both before and after the mainshock (see discussion above). The five chosen eGf events show very similar waveforms to each other, especially in the *P* components (Fig. S5).

The final estimate of radiated energy for all eGf events is 2.19×10^{17} J, with a scaled energy of 2.09×10^{-5} and apparent stress of 0.81 MPa (Table 4). On average, <20 % of the energy is extrapolated into the low frequencies, and in the cumulative fractional energy, the mainshock spectra look fairly Brune-like (Fig. S6a-b). The azimuthal dependence of radiated energy is not as strong as that of some of the other great events, but we do see a local maximum near 150°, along strike to the south (Fig. S6c–d).

4.5. 2007 M_w 8.5 Bengkulu

The 2007 M_w 8.5 Bengkulu event occurred south of the 2005 Nias along the trench, and just off shore of the town of Bengkulu. The rupture occurred in two distinct patches along strike, over 100 s (Konca *et al.* 2008). The rupture plane was 100 × 200 km, striking about 330°, similar to the 2005 Nias and 2004 Sumatra events. For this mainshock, we considered 12 potential empirical Green's function events, ranging from M_w 6.3 to M_w 7.9, but choose to use four, and discard those with different mechanism or magnitude too large or small (see discussion above). The four eGf events and the mainshock have very similar waveforms, as shown at station MDJ (Fig. S7), comparable to the Nias mainshock and eGf events.

The corrected source spectra show a large hole at about 100 s (Fig. S8a). This is likely due to the rupture occurring in two distinct bursts, one represented by a spectrum with a higher corner frequency, and one with a lower corner frequency, so that the interference of the two yields the spectral hole we observe. This peculiar feature shows up in the cumulative fractional energy, so that the amount extrapolated is very low, <10 % on average.

We find an average radiated energy of 1.33×10^{17} J, with $E_R/M_o = 1.98 \times 10^{-5}$, and $\tau_a = 0.77$ MPa (Table 5). The azimuthal distribution of energy is not as pronounced as for the other great events, but there is a slight peak to the north, between 300° and 50° (Fig. S8c–d). We also note that the *P* wave spectra show consistently higher energy values than the *S* waves.

4.6. 2012 M_w 8.6 Off-Sumatra

The 2012 M_w 8.6 off-Sumatra earthquake is the largest strike slip event ever recorded, occurring deep (~40 km) in an intraplate region off of the north coast of Sumatra (McGuire and Beroza 2012; http://www.globalcmt.org/) (Fig. 1a). The region between the Sunda trench, the location of three of the thrust events discussed here, and the Ninety-East ridge is a zone of distributed seismicity that may be associated with a wide diffuse plate boundary bisecting the Indo-Australian Plate (Royer and Gordon 1997). Back projection results indicate that the M_w 8.6 ruptured along several NW–SE and NE–SW trending orthogonal faults, deep in the oceanic lithosphere, spanning a fault surface of about 400 × 300 km total (Meng *et al.* 2012). The following M_w 8.2 aftershock occurred along the southern portion of these faults. Whether this oceanic strike-slip event has implications for the maximum size of continental faulting is an interesting topic of conversation.

We use a magnitude 7.2 event from January 2012 for an eGf, as the aftershocks of ~M 6.2 are too close to the noise level to use teleseismically, yielding a lower energy estimate. From the M_w 7.2 eGf, we estimate an azimuthally averaged radiated energy of 6.71×10^{17} J, and apparent stress of 3.07 MPa, about five times more energetic than the five thrust events (Tables 6 and 7). There is no discernable azimuthal pattern to the radiated energy (Fig. S10c–d), but given that the rupture occurred bilaterally on multiple, conjugate fault planes, we should not expect much directivity overall.

Table 7

Radiated energy for all five great earthquakes, compared to estimates from other studies. The log_{10} 95% confidence intervals in energy from previous tables are translated into apparent stresses, τ_a.

Event	Radiated energy, E_R (J $\times 10^{17}$)					E_R/M_o ($\times 10^{-5}$)	τ_a (MPa)		
	Newman[a, b]	Lay[c]	USGS[d]	This study	This study[e]		Mean	Min	Max
2011 Tohoku-Oki	4.2[a]	4.18	5.1	7.06	4.22	1.57	0.61	0.57	0.65
2004 Sumatra	8.2[b]	2.98	1.1	7.25	4.33	1.12	0.43	0.40	0.46
2010 Maule	2.6[b]	2.10	0.47	1.86	1.11	1.03	0.40	0.38	0.43
2005 Nias	1.1[b]	0.82	0.37	2.19	1.31	2.09	0.81	0.78	0.84
2007 Bengkulu	0.69[b]	0.44	0.26	1.33	0.79	1.98	0.77	0.73	0.81
2012 Off-Sumatra	2.1[a]	n/a	2.7	6.71	4.01	7.89	3.07	2.40	3.93

[a] http://geophysics.eas.gatech.edu/anewman/research/RTerg/

[b] Convers and Newman (2011)

[c] Lay *et al.* (2012)

[d] As reported on http://earthquake.usgs.gov, following Boatwright and Choy (1986)

[e] Based on differences in material parameters, estimates from this study would be 1.67 times larger that those of Newman, so we provide the comparison of our results/1.67

5. Constant Scaled Energy and Apparent Stress

We find that the scaled energy of the six great earthquakes is similar in size to the scaled energy for smaller earthquakes. The scaled energy of all five events is between ~ 1 and 2×10^{-5}, corresponding to an apparent stress of 0.4–0.8 MPa, and the strike-slip off-Sumatra earthquake has apparent stress of ~ 3 MPa. These apparent stresses are well within the range of global values, and the mechanism dependence is consistent with the notion of an immature strike-slip event in cold lithosphere vs. thrust faulting on mature subduction boundaries.

We compare our results to other studies (Convers and Newman 2011; Lay *et al.* 2012; NEIC reported radiated energy, http://earthquake.usgs.gov; Boatwright and Choy 1986) in Table 7. These studies make attenuation, source, and station corrections to teleseismic *P* waves to estimate source spectra and radiated energy. Results from our study compare well with those of Convers and Newman (2011) and Lay *et al.* (2012). With the exception of the 2011 Tohoku-Oki event, the USGS estimates are systematically much lower than the others, as also noted by Newman and Okal (1998) and Di Giacomo *et al.* (2010). This discrepancy is potentially caused by too short a time window in the NIEC analysis. Although we use the same value of ρ as Convers and Newman (2011), their use of $\alpha = 7{,}000$ m/s and a *S*-to-*P* wave partitioning factor of 15.6 actually implies that their values should be 1.67 times smaller than ours. To clarify this comparison, Table 7 also shows the results of this study divided by 1.67. Then, the radiated energies are even more similar from our results. However, there are still sources of uncertainty between the different methods, such as how different station energies are averaged, that could account for the differences between the studies. That our teleseismic eGf deconvolution yields radiated energy results in agreement with other studies validates this method, and demonstrates that it can be used to estimate robust source spectra and other source parameters derived from it. An inherent advantage of eGf techniques is that specific source and attenuation information is not required, and the result is only dependent on the eGf assumptions. We also show that *S* waves, in addition to *P* waves, can be used in teleseismic energy calculation for great earthquakes, which greatly increases the number of records that can be analyzed. For smaller events, the increased attenuation of *S* waves may not allow the same calculation at teleseismic distances.

Convers and Newman (2011) study 342 global earthquakes with $M > 6.5$, and find an average scaled energy, $E_R/M_o = 1.82 \times 10^{-5}$ for thrust events, and 3.63×10^{-5} for strike-slip earthquakes. For our

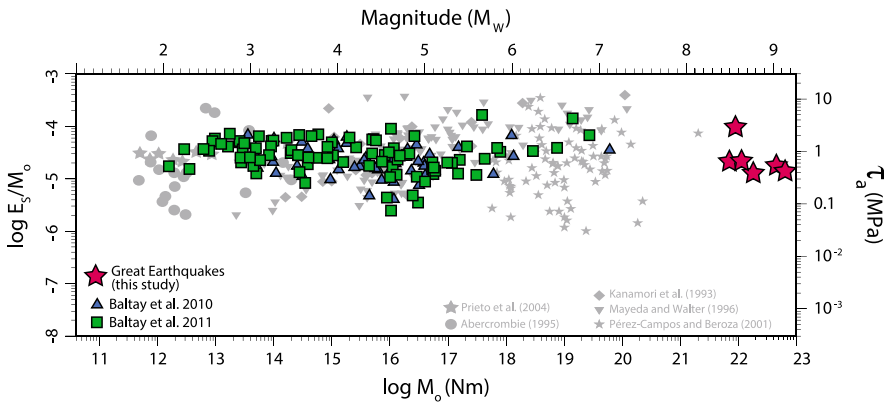

Figure 6
Scaled energy and apparent stress of the six great earthquakes (*red stars*) overlain on the figure of Ide and Beroza (2001) compiling many other studies. Also shown are the scaled energy results from Baltay *et al.* (2010) from the western US, and Baltay *et al.* (2011) from Honshu, Japan. The energy of great earthquakes is consistent with that of other earthquakes, from ~M 2 to M 7. Apparent stress is similar and between 0.4 and 0.8 MPa for the five thrust events, and higher for the 2012 off-Sumatra strike-slip event

sample size of only six earthquakes, it is problematic to determine a difference between mechanisms, yet the factor of ~5 difference between the thrust events and the 2012 Sumatra strike slip event is consistent with Pérez-Campos and Beroza (2001) between those mechanisms for a much larger data set of somewhat smaller earthquakes.

Figure 6 compares our results for scaled energies to previous studies of Baltay *et al.* (2010) and (2011), who used a local empirical Green's function technique to find scaled energy of ~200 events in the western United States and eastern Honshu, Japan, ranging from magnitude ~2 to ~7. Inclusion of the six recent great earthquakes emphasizes the lack of dependence of scaled energy on moment, as these observations show no systematic variation in apparent stress with magnitude.

6. *Azimuthal Dependence of Radiated Energy*

We investigate the azimuthal variations of radiated energy from the six great earthquakes. Because the eGf events are much smaller compared to the mainshock, directivity in the mainshock at long periods should be preserved in measurements of the radiated energy. We see the strongest azimuthal dependence and clearest trends for the largest events, 2004 M_w 9.1 Sumatra and 2011 M_w 9.0 Tohoku-Oki. The other three thrust events also show azimuthal variation of radiated energy, but the patterns are not as well resolved. The 2012 M_w 8.6 off-Sumatra earthquake shows little azimuthal variation, likely due to the fact that it includes complex rupture on multiple perpendicular fault planes. In all cases, although the initial waveforms are quite different; the *P* and *S* components show similar trends, which implies that the relative differences between mainshock and eGf events is the same regardless of the component of motion (Fig. 7).

In the Tohoku-Oki case, we find an energy peak in the strike direction at ~200°, a small peak in the anti-strike direction (along-strike in the opposite direction) at ~20°, and a low near ~100°. Based on the spatio-temporal slip inversion of Ide *et al.* (2011), we interpret the peaks at 200° and 20° to be generated by high apparent velocity along and parallel to the trench as the rupture reaches the trench. The minimum in radiated energy at 100° is in the up-dip, trench direction, which is explained by the observation of high-frequency energy, >0.1 Hz, generated from the down dip (~270°) area, so that the low-frequency energy in the trench-ward direction doesn't contribute much to the overall broadband radiated energy estimated here.

Because of the extended, 1,300 km long rupture of the 2004 Sumatra earthquake, and the strong unilateral rupture propagation for that event, we expect

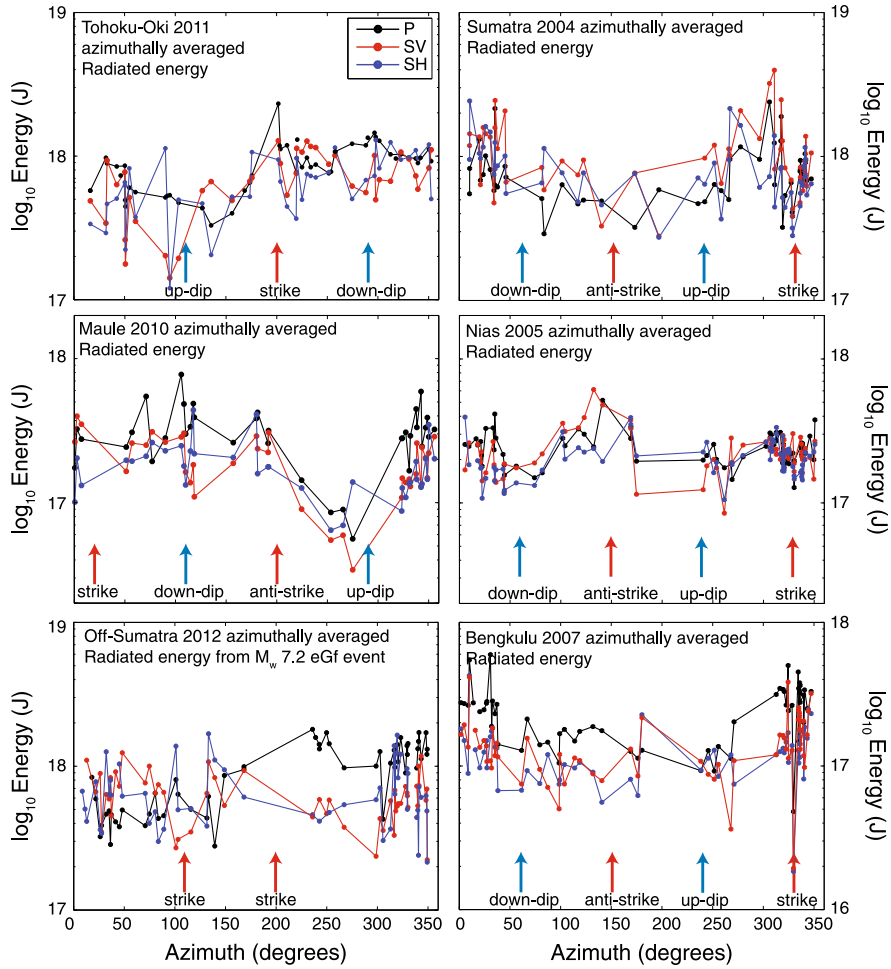

Figure 7
Azimuthal dependence of radiated seismic energy all six great earthquakes, shown as the $\log_{10}$ mean overall eGf corrections, for each component. "Strike" indicates direction or rupture propagation, while "anti-strike" is along the strike in the opposite direction

directivity along strike, towards the north (Ammon *et al.* 2005). We see this clearly in the radiated energy, with a strong peak just west of the 330° strike. In addition, there is a minimum of radiated energy in the anti-strike direction, at ∼150°, which is also explained by the northward rupture directivity. In contrast to the Tohoku-Oki event, which occurred on a compact fault plane with rupture moving up- and down-dip, the 2004 Sumatra event started in the south and moved unilaterally to the north, along strike.

The 2010 M_w 8.8 Maule earthquake shows a strong minimum of radiated energy to the west, at about 250°, and a slight peak to the east, near ∼90°. The other azimuths show fairly constant radiated energy. The rupture started in the south, with a concentration of slip near the epicenter, and then moved to the north with another concentration of high slip (Kiser and Ishii 2012). The minimum in radiated energy to the west is in the trench-ward direction, and in that sense our observations are similar to the minimum in energy seen in the up-dip direction for the Tohoku-Oki earthquake.

Both the 2005 M_w 8.7 Nias and 2007 M_w 8.5 Bengkulu earthquakes show weaker azimuthal variation in radiated energy, perhaps due to their smaller size. The Nias earthquake consisted of bilateral rupture, to the north at 330° and to the south at 150° (Konca *et al.* 2007). We find peaks in radiated energy in these two directions, with a stronger peak to the south, consistent with the larger slip patch in the

southern portion. The Bengkulu rupture also occurred in two distinct south and north patches, but with rupture direction to the north only. In the radiated energy, we resolve only a broad peak in the northerly, along-strike direction.

The 2012 off-Sumatra strike-slip event shows no distinct azimuthal variation in radiated energy; however, this lack of directivity is attributable to rupture on multiple, orthogonal fault planes (MENG *et al.* 2012).

We can discern general source rupture characteristics from the radiated energy. The larger events show stronger azimuthal variation. If radiated energy estimates are to be used for rapid response (see discussion below), then the possibility of variations in single-station estimates due directivity must be taken into account. When paired with a time dependent slip inversion, we can interpret the maxima and minima in energy as particular rupture processes. VENKATARAMAN and KANAMORI (2004) conclude that directivity for dip-slip events with rupture propagating along strike is less than a factor of two at teleseismic distances. However, even for the 2005 Nias and 2007 Bengkulu events, which show the smallest directivity, we see at least a factor of two difference in the radiated energy between stations. The 2004 Sumatra earthquake, which does propagate along strike, shows nearly an order of magnitude difference of energy from station to station. FAVREAU and ARCHULETA (2003) forward modeled the energy radiated by the 1979 Imperial Valley earthquake, and found extreme directivity from the super-shear rupture, with 86 % of the energy radiated in the along-strike direction. Therefore, it is essential to take variability in energy due to directivity into account when estimated radiated energy teleseismically. With our method, we calculate energy at many stations, and take an azimuthally weighted average to account for the directivity. Expressing the uncertainty in estimates of radiated energy becomes imperative for rapid response; in cases of extreme directivity, the measure of radiated energy could be off by an order of magnitude depending on the stations considered. In an unlucky case where the early data is from the direction of negative directivity, the underestimation of energy would present an unrealistically enervated view of a potentially devastating earthquake.

7. *Real-Time Determination of Radiated Energy*

Radiated seismic energy is a fundamental earthquake source parameter, and reflects both the amount of material displaced and the speed at which that occurs. Earthquakes radiating greater amounts of energy per unit fault area are expected to produce larger ground motion, and the high frequency energy content of earthquakes can greatly affect the built environment. On the other hand, earthquakes that have a low ratio of radiated energy to seismic moment release energy more slowly and have the potential to create anomalously large tsunami for their size (NEWMAN and OKAL 1998). Rapid determination of radiated energy as a dynamic measure of the earthquake size could aid in hazard mitigation efforts or rapid emergency response, and could quickly indicate if an earthquake will generate unusually large tsunami amplitudes, or will likely cause large ground shaking.

During the 2011 Tohoku-Oki earthquake, the Japanese early warning and information systems worked well, as many Japanese were warned of ground shaking and tsunami waves before their arrival. However, SAGIYA *et al.* (2011) noted that although the system worked well, more accurate, quick determination of source parameters would increase the efficacy of all of the systems, and in any case redundancy from independent real-time hazard assessment would have great value. Tsunami are generated most strongly at the shallowest part of rupture (i.e., at the trench), which is typically far enough offshore, that even local tsunami will take up to 30 min to arrive, so a rapid assessment of the radiated energy from an earthquake made within $\sim$10 min would still allow 20 min of warning.

We propose that our method could be used for rapid energy estimation to support other ongoing approaches. A global eGf database could be set up so that the largest global earthquakes can quickly be analyzed after their occurrence. Given a magnitude difference of 1.5 magnitude units between the eGf and the mainshock and our eGf magnitude limit of $\sim$6.5, we surmise that the smallest earthquake that could be studied teleseismically with our method is about M 8. Figure 8 shows the distribution of magnitude 6.5 and greater earthquakes globally for the

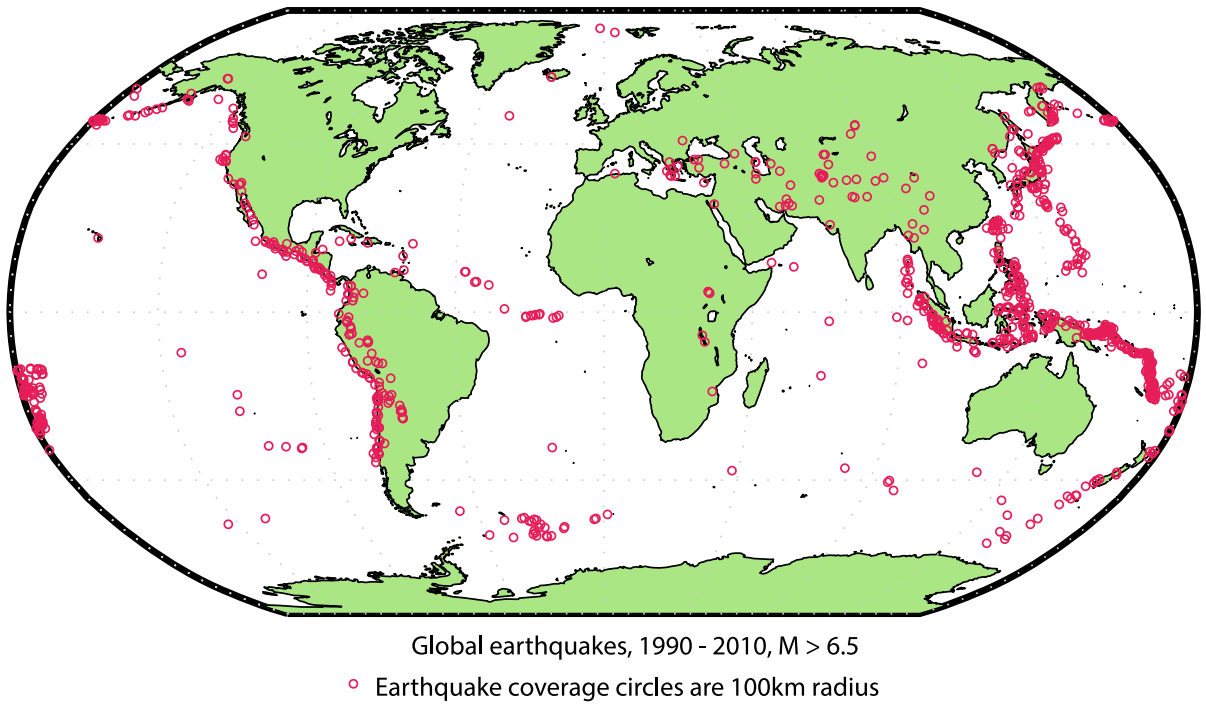

Figure 8
Global earthquakes > M6.5 from 20 years (1990–2010). Each earthquake is shown as a *circle* of radius 100 km, which we find to be the approximate radius of influence of eGf events. Mainshocks occurring within a *circle* can be corrected acceptably well by eGf deconvolution to estimate radiated energy

20-year period (1990–2010). Each earthquake is shown as a circle of radius 100 km, which we found to be the most effective range of eGf events for mainshock deconvolution. Hence, any $M \geq 8$ mainshock located within any 100 km radius circle could be studied with our method. There is dense coverage of $M_w > 6.5$ earthquakes along most of the world's subduction zones, where we expect the largest future hazardous earthquakes are most likely to occur. Regions such as the Mediterranean, San Andreas Fault system, and the Himalayan system have sparser coverage, so energy estimation using eGfs would not be as rapid. The radius over which the eGf deconvolution is robust and stable, however, would be frequency dependent. Because smaller events have proportionally more of their energy at shorter periods, where there is more anelastic attenuation, the correction may only work at shorter distances.

Potential eGf earthquakes, as shown in Fig. 8, recorded at reliable GSN stations would be prescreened and pre-processed (quality checked, windowed and tapered), and their three-component spectra stored in the database. Once a large earthquake occurs, it could quickly be located and matched with appropriate eGf events. Our energy estimation method is not computationally intensive, so the mainshock energy could be determined rapidly. The time consuming steps are in screening the potential eGf events and determining their parameters, which would be accomplished before the occurrence of a mainshock event, cutting back significantly on the processing time. Then, the radiated energy could be calculated within a few minutes of the arrival of waveforms at a station.

For the closest GSN stations considered here at 30° distance, *P* waves first arrive 6 min after rupture begins, and *S* waves begin to arrive at about 12 min. We have shown that there is no dependence of estimated energy on station distance, so that the closest stations could reliably be used, but for redundancy, at least six stations should be used for the estimation. We have shown that a directivity correction through averaging is important for an accurate result if stations are well distributed in azimuth. Since energy

estimated from P and S waves yields consistent results, the estimation could be performed in real time using only the P arrivals, and then updated as the S waves arrive. Thus, an estimate of radiated seismic energy could be calculated within $\sim$10 min. That number could be reduced if the method is shown to be stable for earthquakes recorded at shorter distances.

Given that most tsunami are generated at the trench, and the propagation time from there to shore is on the order of 30 min, use of this method for quick tsunami potential determination would allow approximately 20 min for evacuation or early warning. Furthermore, the azimuthal energy dependence may quickly inform the rupture model and directivity, which could also be used to improve rapid hazard characterization.

Convers and Newman (2011) developed a method for fast determination of the radiated energy, which was recently implemented as an IRIS Data Management Systems product (http://www.iris.edu/dms/products/eqenergy/). Their method estimates radiated energy teleseimically from averaged attenuation models for the whole earth to account for energy loss, which is dependent on radiation pattern, and hence specific knowledge of the mainshock depth, location and mechanism. Di Giacomo *et al.* (2010) also proposed a similar system for rapid energy determination, using pre-computed numerically simulated Green's functions. They also pointed out the necessity of determining the radiated energy as a dynamic measure of the earthquake's size for rapid earthquake assessment, rather than simply the static moment magnitude.

The limitations of these two methods, as well as our own, include the fact that the data is teleseismic. In all cases, the size of the smallest event that can be analyzed is limited, although the method of Convers and Newman (2011) and Di Giacomo *et al.* (2010) are able to analyze smaller events than our proposed method. Secondly, the waves must travel a far distance from the source to the station before the energy can be estimated, which automatically delays the rapidity of the estimate; however, teleseismic methods are very valuable when there are few local stations, as is the case in some subduction zones, or when local stations go off-scale or off-line, which happened during the 2011 Tohoku-Oki event.

Our method has its own limitations, in that we need a priori moment, and the eGf events have to be computed from real data. However, rapid moment magnitude determinations are now routinely made, so they could be implemented into our method. The use of real eGf events implies that any heterogeneity in the earth structure near the source or site, or along the travel path, will automatically be accounted for, unlike in the other methods.

On the other hand, because our method is empirical and not specifically dependent on the mechanism, we could simultaneously run deconvolution with many potential eGf events, and find a converging best answer as more information arrives about the large earthquake. As well, although we have not tested the method for deep events, it is likely that they will not pose a large problem if appropriate eGf events of similar depth are used, while the approach of Convers and Newman (2011) cannot handle deep events without corrections to the assumed attenuation structure.

In any case, redundancy from independent real-time hazard assessment would have great value as we work towards mitigating the effects of great earthquakes. There is still work to be done to get these rapid energy estimates to be implemented for tsunami warning, and hence all possible approaches and information should be taken into account.

8. Conclusions

We expand on the teleseismic empirical Green's function deconvolution approach, using eGf events as large as M_w 7.4. We show that both P and S waves can be used in the eGf deconvolution teleseismically to give consistent energy estimates, whereas before, primarily only P waves were used at teleseismic distances (e.g. Boatwright and Choy 1986).

We find that radiated energy of six great earthquakes is consistent with the self-similar source physics seen for smaller events. The scaled energy of each of the thrust events is in the range 1–2 $\times$ 10^{-5}, and apparent stress ranges from 0.4 to 0.8 MPa. The great strike-slip 2012 off-Sumatra event has a higher apparent stress of 3 MPa. These values are very consistent with those found for a wide range of

events, ranging from micro-earthquakes to other subduction zone megathrust earthquakes. Our results support a mechanism dependence on radiated energy, as has been found in previous studies, between energetic strike-slip (particularly oceanic lithospheric faulting) and enervated subduction zone thrust faulting. Our estimates of radiated energy for each event are similar to those of other researchers.

We demonstrated that teleseismic eGf deconvolution is robust and stable method for removing path and site effects using both *P* and *S* waves, to measure radiated seismic energy. EGF deconvolution could thus be used in other teleseismic applications to isolate source spectra or time series. Ide *et al.* (2011) used teleseismic eGf deconvolution to invert for a spatio-temporal slip distribution of the 2011 Tohoku-Oki earthquake, a method that could be applied to the great earthquakes we have analyzed here as well.

The azimuthal distribution of radiated energy is consistent with the sense of rupture propagation for each earthquake. The larger events show stronger and more varied directivity in energy, which can be interpreted as high apparent velocity along the trench, and slow rupture in the direction towards the trench. The smaller events show azimuthal dependence of energy as well, so that directivity effects should be considered when estimating radiated energy from teleseismic data for great earthquakes. Further work to couple time-dependent rupture propagation with the energy radiation may further illuminate source characteristics of megathrust earthquakes.

Acknowledgments

IRIS Standing Order of Data (SOD) (Owens *et al.* 2004) was used to acquire Global Seismic Network (GSN) data. The authors thank Jesse Lawrence for help with acquiring GSN data and use of SOD. The authors thank Adrien Oth, Kevin Mayeda and Lusi Rivera for organizing and convening the workshop "Earthquake source physics on various scales," and ECGS for hosting. We also thank two anonymous reviewers and the guest editor, Adrien Oth, for their constructive comments and reviews which improved the manuscript. A. Baltay was partially supported at Stanford by a Gabilan Stanford Graduate Fellowship, as well as through financial support from Pacific Gas and Electric.

References

Abercrombie, R. E. (1995), *Earthquake source scaling relationships from −1 to 5* M_L *using seismograms recorded at 2.5-km depth*, J. Geophys. Res., *100*(B12), 24015–24036, doi:10.1029/95JB02397.

Abercrombie, R. E. (2013), *Comparison of direct and coda wave stress drop measurements for the Wells, Nevada, earthquake sequence*, J. Geophys. Res., *118*, doi:10.1029/2012JB009638.

Ammon, C. J., A. A. Velasco and T. Lay (1993), *Rapid estimation of rupture directivity: application to the 1992 Landers (MS = 7.4) and Cape Mendocino (Ms = 7.2), California earthquakes*, Geophy. Res. Lett., *20*(2), 97–100.

Ammon, C. J., C. Ji, H.-K. Thio, D. Robinson, S. Ni, V. Hjorleifsdottir, H. Kanamori, T. Lay, S. Das, D. Helmberger, G. Ichinose, J. Polet and D. Wald (2005), *Rupture Process of the 2004 Sumatra-Andaman Earthquake*, Science, *308*(5725), 1133–1139. doi:10.1126/science.1112260.

Aster, R. C., D. E. McNamara, and P. D. Bromirski (2008), *Multidecadal climate-induced variability in microseisms*, Seismo. Res. Lett., *79*(2):194–202.

Baltay, A., G. Prieto and G. C. Beroza (2010), *Radiated seismic energy from coda measurements and no scaling in apparent stress with seismic moment*. J. Geophys. Res. 115, B08314.

Baltay, A., S. Ide, G. Prieto, and G.Beroza (2011), *Variability in earthquake stress drop and apparent stress*, Geophys. Res. Lett., *38*, L06303, doi:10.1029/2011GL046698.

Banerjee, P., F. F. Pollitz, and R. Burgmann (2005), *The size and duration of the Sumatra-Andaman earthquake from far-field offsets*, Science, *308*, 1769–1772.

Billham, R. (2005), *A flying start, then a slow slip*, Science, *308*, 1126–1127.

Boatwright, J. and G. Choy (1986), *Teleseismic estimates of the energy radiated by shallow earthquakes*, J. Geophys. Res., *91*, 2095–2112.

Bormann, P., and D. Di Giacomo, (2011), *The moment magnitude* M_w *and the energy magnitude* M_e*: common roots and differences*, Journ. of Seismol., *15*(2), 411–427.

Chlieh, M., J-P. Avouac, V. Hjorleifsdottir, T-R A. Song, C. Ji, K. Sieh, A. Sladen, H. Hebert, L. Prawirodirdjo, Y. Bock, and J. Galetzka (2007), *Coseismic Slip and Afterslip of the Great Mw 9.15 Sumatra-Andaman Earthquake of 2004*, Bull. Seismol. Soc. Am., *97*, 152–173.

Choy, G. L., and J. L. Boatwright (1995), *Global patterns of radiated seismic energy and apparent stress*, J. Geophys. Res., *100*, 18,205–18,228.

Choy, G. L., A. McGarr, S. H. Kirby and J. Boatwright (2006), An overview of the global variability in radiated energy and apparent stress, in *Earthquakes: Radiated energy and the physics of faulting*, Geophysical Monograph Series, *170*, 43–57, doi:10.1029/170GM01.

Convers, J. A., and A. V. Newman (2011), *Global evaluation of large earthquake energy from 1997 through mid-2010*, J. Geophys. Res., *116*, B08304, doi:10.1029/2010JB007928.

Courboulex, F., Virieux, J., Deschamps, A., Gibert, D. and Zollo, A. (1996), *Source investigation of a small event using empirical Green's functions and simulated annealing*. Geophys. J. Int., *125*:768–780. doi:10.1111/j.1365-246X.1996.tb06022.x.

Dean, S.M., L. C. McNeill, T. J. Henstock, J. M. Bull, S. P. S. Gulick, J. A. Austin, Jr., N. L. B. Bans, Y. S. Djajadihardja and H. Permana (2010), *Contrasting decollement and prism properties over the Sumatra 2004–2005 earthquake rupture boundary*, Science, *329*, 207–210.

Di Giacomo, D., S. Parolai, P. Bormann, H. Grosser, J. Saul, R. Wang, and J. Zschau (2010), *Suitability of rapid energy magnitude determinations for emergency response purposes*, Geophys. J. Int., *180*(1): 361–374, doi:10.1111/j.1365-246X.2009.04416.x.

Favreau, P. and R. J. Archuleta (2003), *Direct seismic energy modeling and application to the 1979 Imperial Valley earthquake*, Geophy. Res. Lett., *30*(5), 1198, doi:10.1029/2002GL015968.

Hanks, T. C., and W. Thatcher (1972), *A graphical representation of seismic source parameters*, J. Geophys. Res. *77*, 4292–4405.

Hartzell, S. H. (1978), *Earthquake aftershocks as Green's functions*, Geophys. Res. Lett. *5*(1), doi:10.1029/GL005i001p00001.

Hayes, G. (2010), *Finite Fault Model. Updated Result of the Feb 27, 2010 Mw 8.8 Maule, Chile Earthquake*. http://earthquake.usgs.gov/earthquakes/eqinthenews/2010/us2010tfan/finite_fault.php, (US Geological Survey/NEIC, 2010).

Hough, S. E. (2001), *Empirical Green's function analysis of recent moderate events in California*, Bull. Seismol. Soc. Am., *91*, 456–467.

Ide, S., and G. C. Beroza (2001), *Does apparent stress vary with earthquake size?*, Geophys. Res. Lett., *28*(17), 3349.

Ide, S., G. C. Beroza, S. G. Prejean, and W. L. Ellsworth (2003), *Apparent break in earthquake scaling due to path and site effects on deep borehole recordings*, J. Geophys. Res., *108*(B5), 2271, doi:10.1029/2001JB001617.

Ide, S., A. Baltay and G. C. Beroza (2011), *Shallow dynamic overshoot and energetic deep rupture in the 2001 M_w 9.0 Tohoku-Oki Earthquake*, Science, *332*, 6036, 1426–1429. doi:10.1126/science.1207020.

Ishii, M., P. M. Shearer, H. Houston and J. E. Vidale (2005), *Extent, duration and speed of the 2004 Sumatra-Andaman earthquake imaged by the Hi-Net array*, Nature, *435*, doi:10.1038/nature03675.

Kanamori, H. (1972), *Mechanism of tsunami earthquakes*, Phys. Earth Planet. Inter. *6*, 346–359.

Kanamori, H. (2006), The radiated energy of the 2004 Sumatra-Andaman earthquake, in *Earthquakes: radiated energy and the physics of faulting,* Geophysical Monograph Series, *170*, 59–68, doi:10.1029/170GM10.

Kanamori, H. and J. Given (1981), *Use of long-period surface waves for rapid determination of earthquake-source parameters*. Phys. Earth Planet. Inter. *27*, 8.

Kane, D. L., G. A. Prieto, F. L. Vernon, and P. M. Shearer (2011), *Quantifying seismic source parameter uncertainties*, Bull. Seism. Soc. Am., *101*, 535–543.

Kane, D. L., D. L. Kilb and F. L. Vernon (2013), *Selecting empirical Green's functions in regions of fault complexity; a study of data from the San Jacinto fault zone, Southern California*, Bull. Seismol. Soc. Am., *103*(2A), 641–650, doi:10.1785/0120120189.

Kiser, E. and Ishii, M. (2012), *Combining seismic arrays to image the high-frequency characteristics of large earthquakes*, Geophys. Jour. Inter., *188*:1117–1128. doi:10.1111/j.1365-246X.2011.05299.x.

Konca, A.O., V. Hjorleifsdottir, T-R. A. Song, J.-P. Avouac, D. V. Helmberger, C. Ji, K. Sieh, R. Briggs, and A. Meltzner (2007), *Rupture kinematics of the 2005 Mw 8.6 Nias-Simeulue earthquake from the joint inversion of seismic and geodetic data (in The 2004 Sumatra-Andaman earthquake and the Indian Ocean tsunami)*, Bull. Seismol. Soc. Am., *97*(1A):S307–S322.

Konca, A. O., J-P Avouac, A. Sladen, A. J. Meltzner, K. Sieh, P. Fang, Z. Li, J. Galetzka, J. Genrich, M. Chlieh, D. H. Natawidjaja, Y. Bock, E. J. Fielding, C. Ji and D. Helmberger (2008), *Partial rupture of a locked patch of the Sumatra megathrust during the 2007 earthquake sequence*, Nature, *456*. doi:10.1038/nature07572.

Koper, K. D., Hutko, A. R., Lay, T., Ammon, C. J., and Kanamori, H. (2011). *Frequency-dependent rupture process of the 2011 M_w 9.0 Tohoku Earthquake: Comparison of short-period P wave backprojection images and broadband seismic rupture models*. Earth, planets and space, *63*(7), 599–602.

Lay, T., H. Kanamori, C. J. Ammon, M. Nettles, S. N. Ward, R. C. Aster, S. L. Beck, S. L. Bilek, M. R. Brudzinski, R. Butler, H. R. DeShon, G. Ekstrom, K. Satake, and S. Sipkin (2005). *The great Sumatra- Andaman earthquake of 26 December 2004*, Science *308*, 1127–1133.

Lay, T., C. J. Ammon, H. Kanamori, Y. Yamazaki, K. F. Cheung, and A. R. Hutko (2011), *The 25 October 2010 Mentawai tsunami earthquake (M_w 7.8) and the tsunami hazard presented by shallow megathrust ruptures*, Geophys. Res. Lett., *38*, L06302, doi:10.1029/2010GL046552.

Lay, T., H. Kanamori, C. J. Ammon, K. D. Koper, A. R. Hutko, L. Ye, H. Yue, and T. M. Rushing (2012), *Depth-varying rupture properties of subduction zone megathrust faults*, J. Geophys. Res., *117*, B04311, doi:10.1029/2011JB009133.

Lay, T., Y. Fujii, E. Geist, K. Koketsu, J. Rubinstein, T. Sagiya, and M. Simons (2013), *Introduction to the Special Issue on the 2011 Tohoku Earthquake and Tsunami*, Bull. Seism. Soc. Am., *103*:1165–1170, doi:10.1785/0120130001.

McGuire, J. J. and G. C. Beroza (2012), *A rogue earthquakes off Sumatra*, Science, *336*, 6085, 1118–1119, doi:10.1126/science.1223983.

Meng, L., J.-P. Ampuero, J. Stock, Z. Duputel, Y. Luo and V. C. Tsai (2012), *An earthquake in a maze: compressional rupture branching in a weakened oceanic lithosphere during the April 11 2012 M8.6 Sumatra earthquake*, Science, *337*:6095. doi:10.1126/science.1224030.

Moreno, M., M. Rosenau and O. Oncken (2010), 2010 *Maule earthquake slip correlates with pre-seismic locking of Andean subduction zone*, Nature *467*, 198–202 doi:10.1038/nature09349.

Mori, J. Frankel, A. (1990). *Source parameters for small events associated with the 1986 North Palm Springs, California, earthquake determined using empirical Green functions*, Bull. Seism. Soc. Am. *80*, 278–295.

Newman, A. V., and E. A. Okal (1998), *Teleseismic estimates of radiated seismic energy: The E/M $_0$ discriminant for tsunami earthquakes,* J. Geophys. Res., *103*(B11), 26,885–26,898, doi:10.1029/98JB02236.

Newman, A. V., G. Hayes, Y. Wei, and J. Convers (2011), *The 25 October 2010 Mentawai tsunami earthquake, from real-time*

discriminants, finite-fault rupture, and tsunami excitation, Geophys. Res. Lett., *38*, L05302, doi:10.1029/2010GL046498.

Newman, A. (2011) Real-Time Earthquake Energy and Rupture Duration Determinations, http://geophysics.eas.gatech.edu/anewman/research/RTerg/2011/11031100/, Accessed November 6, 2011.

Owens, T.J., H. P. Crotwell, C. Groves, and P. Oliver-Paul (2004), *SOD: Standing Order for Data*. Seismol. Res. Lett., *75*:515–520.

Pérez-Campos, X., and G. C. Beroza (2001), *An apparent mechanism dependence of radiated seismic energy*, J. Geophys. Res.; *106*, 11,127–11,136.

Perez-Campos, X., S. K. Singh and G. C. Beroza (2003) *Reconciling teleseismic and regional estimates of seismic energy*, Bull. Seismol. Soc. Am. *95*(5), 2123–2130.

Royer, J. Y., and R. G. Gordon (1997). *The motion and boundary between the Capricorn and Australian plates*. Science, *277*(5330), 1268–1274.

Sagiya, T., H. Kanamori, Y. Yagi, M. Yamada, and J. Mori (2011), *Rebuilding seismology*, Nature, *473*, 146–148, doi:10.1038/473146a.

Singh, S. K., and Ordaz, M. (1994). *Seismic energy release in Mexican subduction zone earthquakes*. Bull. Seismol. Soc. Am, *84*(5), 1533–1550.

Suzuki, W., S. Aoi, H. Sekiguchi, and T. Kunugi (2011), *Rupture process of the 2011 Tohoku-Oki mega-thrust earthquake (M9.0) inverted from strong-motion data*, Geophys. Res. Lett., *38*, L00G16, doi:10.1029/2011GL049136.

Venkataraman, A., L. Rivera, and H. Kanamori (2002), *Radiated energy from the 16 October 1999 Hector Mine earthquake: Regional and teleseismic estimates*, Bull. Seismol. Soc. Am., *92*, 1256–1265, doi:10.1785/0120000929.

Venkataraman, A. and H. Kanamori (2004), *Effect of directivity on estimates of radiated seismic energy*, J. Geophys. Res., *109*, B04301, doi:10.1029/2003JB002548.

Wyss, M. and J. Brune (1968), *Seismic moment, stress, and source dimensions for earthquakes in the California-Nevada region*, J. Geophys. Res., *73*(14), 4681–4694, doi:10.1029/JB073i014p0468.

(Received May 13, 2013, revised February 17, 2014, accepted February 19, 2014, Published online April 4, 2014)